Chapter 2

Anharmonic Vibrational Signatures of Peptides — Methods and Applications

Jianping Wang

Additional information is available at the end of the chapter

http://dx.doi.org/10.5772/58888

1. Introduction

Understanding the structure of proteins is a key to understanding their functions. Infrared (IR) spectroscopy is a very sensitive tool for studying three-dimensional molecular structures of proteins [1,2] in conditions relevant to biology, for example, in solution phase. This is because the vibrational frequency is determined by the chemical structure of the chromophore. However, both intra- and intermolecular force fields are involved. For the intramolecular aspect, the frequency of a specific vibration is influenced by the collective interaction of this mode with the rest 3N-7 (or 3N-6 for linear molecule) modes, where N is the total number of atoms in the molecular system. As for the intermolecular aspect, the frequency of a specific vibration is also influenced by its neighboring solvent molecules. Further, the IR spectroscopy is essentially a label-free method. There are a variety of intrinsic vibrational modes that can be used to characterize protein structures, thus the use of external chromophore, as is obligatory in some other spectroscopic methods, is not absolutely necessary for the IR method.

Commercial Fourier-transform infrared (FTIR) spectrometer allows the measurement of the IR absorption spectra for a large number of vibrational transitions in proteins in the mid-IR frequency range (4000 – 650 cm^{-1}). Certain key vibrational modes are well studied, and empirical relationship between their frequency and protein structure has been established. A well-known example of such is the amide-I mode, which is mainly the C=O stretching vibration. It is usually used as a protein/peptide backbone conformational reporter, because the amide unit is the linkage between amino acid residues and appears periodically on the peptide chain. The well-known linear IR signature of the α-helix, although appears to be a single absorption peak at 1640-1658 cm^{-1}, has a two-component (a low-frequency A-mode and a high-frequency E-mode) band structure [3]. For the anti-parallel β-sheet, there is a major sharp absorption band appearing at 1620-1640 cm^{-1} and a weak peak at 1680-1696 cm^{-1} [4-8],

while the parallel β-sheet only exhibits a major sharp absorption band at 1620-1640 cm^{-1} [6,8,9]. Whereas the IR signature of other conformations, such as the β-turn and random coil, usually appears to be a single band at 1640-1658 cm^{-1} for random coil, or at higher frequency for the β-turn.

Assuming a harmonic potential, quantum chemical calculations can yield a complete set of vibrational frequencies of mid-sized polypeptide molecules. Good performance of the Kohn-Sham formulation of density functional theory (DFT) for predicting molecular geometries and harmonic vibrational frequencies has been established. For example, the fundamental vibrational frequencies for nine amide modes (amide-I to -VII, and amide-A and -B) in simple peptides using the hybrid density functional B3LYP are found to be in reasonable agreement with measurements in the gas phase. In certain cases the results are even better than those from strictly *ab initio* approaches, such as second-order Moller-Plesset perturbation theory (MP2) [10]. However, because of the crudeness of the harmonic approximation, a frequency scaling factor is often needed in order to better match the theoretical prediction with experimental measurement. The frequency scaling factor is dependent on the level of theory used. A typical scaling factor is 0.9914 at the level of B3LYP/6-31G(d) [11]. However, a single scaling factor cannot scale multiple vibrational frequencies satisfactorily for a given molecule.

In reality, molecular vibrations are intrinsically anharmonic. Because of this, experimentally measured IR spectra are often complicated: it contains not only absorption peaks coming from fundamental transitions, but also those from overtone and combination transitions. For a given vibrational chromophore, the frequency difference between its fundamental transition and its overtone transition is known as the (diagonal) anharmonicity. For a pair of vibrational chromophores, the frequency difference between the sum of their fundamental transitions and that of the combinational transition is known as the off-diagonal anharmonicity. The measurement and assignment of overtone and combination bands in conventional linear IR spectroscopy have been known to be trouble some. This is because for the low-frequency modes, their overtone and combination bands fall into the high-frequency region that could be already very crowded; and for the high-frequency modes, their overtone and combination bands will fall into the high-frequency region of the mid-IR or even into the near-IR regime.

Using the two-dimensional infrared (2D IR) spectroscopy developed in recent years, measurement of anharmonic frequencies in the mid-IR region has been made easier. In this method, a typical two-frequency 2D IR spectrum containing a set of anharmonic vibrators can be obtained, and from which the anharmonic frequencies, diagonal- and off-diagonal anharmonicities can be measured.

With the aid of modern laser technology, 2D IR spectroscopic studies in the 3-μm wavelength region (frequency = 3300 cm^{-1}) [12], 4-μm (2500 cm^{-1}) [13], 5-μm (2000 cm^{-1}) [14-17], 6-μm (1666 cm^{-1}) [18-20] and 8-μm (1250 cm^{-1}) [21] have been reported. This method is expected to be more powerful with the use of broadband laser sources in the future. Further, the 2D IR spectroscopic method also allows additional anharmonic vibrational parameters to be acquired, for example, diagonal and off-diagonal anharmonicities, and anharmonic couplings. Recent studies have shown that these parameters are also sensitive to molecular structures. In addition, the distributions of these vibrational parameters can also be experimentally determined by 2D IR.

http://dx.doi.org/10.5772/58888

It is of great importance to computationally predict the anharmonic vibrational properties of biomolecules, so that they can be used to interpret experimental IR results. The second-order perturbative vibrational treatment (PT2) [22,23] allows such computations. In this method, a full cubic and a semidiagonal quartic force field is obtained by central numerical differentiation of analytical second derivatives [24]. Un-scaled anharmonic vibrational frequencies of medium size molecules can be obtained quite efficiently. A previous study [25] has shown that the performance of B3LYP functional with reasonable basis sets in computing anharmonic vibrational frequencies of semirigid molecules is quite satisfactory. In addition, high-performance computer clusters can be utilized to compute the cubic and quartic derivatives for a given molecular system so that the anharmonic vibrational frequencies can be obtained efficiently using the DFT/PT2 combination. Very recently, the chain-length dependent anharmonicity and mode-delocalization of the amide-I mode [26], and that of the amide-A mode [27], in typical peptide conformations, have been reported.

In this chapter, we present a review of our recent works in studying the anharmonic vibrations of peptide oligomers. Methods to predict the anharmonic parameters are reviewed followed by results and discussions, mainly on the amide-I modes of peptides. The conformational dependence of the obtained anharmonic parameters is discussed. Results are useful in gaining more insights into the structural basis of the anharmonic vibrations of proteins and peptides.

2. Methods

2.1. Anharmonic vibrational frequency and anharmonicity

In the normal mode picture, the vibrational energy of fundamentals, overtones and combination bands for an N-atom molecular system can be generally written in the following form:

$$E\left(n_i, n_j\right) = E_0 + hc\sum_{i}^{3N-6}\omega_i\left(n_i+\frac{1}{2}\right) + hc\sum_{i\le j}^{3N-6}x_{ij}\left(n_i+\frac{1}{2}\right)\left(n_j+\frac{1}{2}\right), \tag{1}$$

where ω_i is the harmonic frequency, n_i is the vibrational quantum number of the ith mode, x_{ij} is the anharmonic correction term. Applying the perturbation theory to the second-order [22-24], one can obtain x_{ij} in terms of the cubic and quartic force constants. The resulting anharmonic fundamental, the overtone and the combination band frequencies are $\nu_i=\omega_i+2x_{ii}+\frac{1}{2}\sum_{j\neq i}x_{ij}$, $\nu_{2i}=2\nu_i+2x_{ii}$ and $\nu_{ij}=\nu_i+\nu_j+x_{ij}$ respectively, from which one obtains the diagonal anharmonicity: $\Delta_{ii}=2\upsilon_i-\upsilon_{2i}=-2x_{ii}$, and the mixed-mode off-diagonal anharmonicity $\Delta_{ij}=\upsilon_i+\upsilon_j-\upsilon_{ij}=-x_{ij}$. The diagonal anharmonicity can be written as [22-24]:

$$\Delta_{ii}=\frac{1}{8}\left[-\Phi_{iiii}+\frac{5\Phi_{iii}^2}{3\omega_i}+\sum_{k\neq i=1}^{3N-7}\frac{\Phi_{iik}^2\left(8\omega_i^2-3\omega_k^2\right)}{\omega_k\left(4\omega_i^2-\omega_k^2\right)}\right]. \tag{2}$$

The first two terms of equation (2) incorporates exclusively energy derivatives with respect to the *i*th mode whose diagonal anharmonicity is being considered. The coefficients Φ_{ijk} and Φ_{ijkl} are the third and fourth derivatives of the potential that involve other normal coordinates. The off-diagonal anharmonicity for any two vibrators *i* and *j* can also be expressed in terms of the cubic and quartic force constants and harmonic frequencies:

$$\Delta_{ij} = \frac{1}{4}\left(-\Phi_{iijj} + \frac{\Phi_{iii}\Phi_{ijj}}{\omega_i} + \frac{\Phi_{jjj}\Phi_{iij}}{\omega_j} + \frac{2\Phi_{iij}^2\omega_i}{4\omega_i^2 - \omega_j^2} + \frac{2\Phi_{jji}^2\omega_j}{4\omega_j^2 - \omega_i^2} \right) + \frac{1}{4}\sum_{k\neq j\neq i=1}^{3N-8}\left[\frac{\Phi_{iik}\Phi_{jjk}}{\omega_k} - \frac{2\Phi_{ijk}^2\left(\omega_i^2 + \omega_j^2 - \omega_k^2\right)\omega_k}{\omega_i^4 + \omega_j^4 + \omega_k^4 - 2\left(\omega_i^2\omega_j^2 + \omega_i^2\omega_k^2 + \omega_j^2\omega_k^2\right)} \right]. \quad (3)$$

The first bracket contains the interaction between mode *i* and *j*, while the second line is due to the interaction of mode *i* and *j* with the remaining *3N-8* modes. In addition, the composition of Δ_{ii} and Δ_{ij} can be examined for a given vibrational mode to investigate the localization degree of the anharmonic forces [28]. Examples of such calculations have been given previously [24,29,30].

2.2. Anharmonic vibrational coupling and local modes

The through bond and through space interactions amongst vibrational chromophore units cause the anharmonic vibrational excitations to exchange from site to site. This is the physical origin of vibrational coupling. There are several ways to assess the vibrational coupling. The first approach is through *ab initio* computations. Wavefunction de-mixing of a *N*-unit coupled system can yield *N* local mode frequencies and 1/2*N*(*N*-1) bilinear couplings [29]. This method is ideal for a collection of vibrational chromophores of the same kind. Taken the amide-I mode for example, a collection of normal modes can be treated as a linear combination of uncoupled local modes, whose mixing angle ξ defined below can be obtained from the normal mode eigenvectors [29]:

$$\xi = 1/2 \cdot \tan^{-1}[2|\beta_{ij}| / (\nu_i^0 - \nu_j^0)], \quad (4)$$

where β_{ij} is the coupling of two local states with frequencies ν_i^0 and ν_j^0. Normal-mode displacement in the basis of the entire 3*N*-6 normal modes can be obtained by a frequency calculation, from which the vibrational wave functions of the amide-I normal mode in the reduced normal mode basis can be reconstructed. For the amide-I modes in a peptide system such a calculation is straightforward if the mode is assumed to be mainly a C=O stretching vibration. In this way an *N* by *N* matrix (thus a reduced amide-I subspace from the entire 3*N*-6 normal modes) was obtained for a system containing *N* amide units. Through such a procedure, the transition frequency of the local modes, the wave function mixing angle, and intermode coupling are obtained together. This method is particularly useful for assessing the coupling strength between the nearest neighboring chromophores that are covalently-bonded.

http://dx.doi.org/10.5772/58888

The second approach is to use transition multipole interaction. Bilinear term in the expansion of the normal mode displacement of vibrational oscillator is the lowest order of the through space interaction potential [3]. The couplings can be evaluated conveniently either by using an electrostatic transition dipole coupling (TDC) scheme [31,32], or using the transition charge and charge flux interaction [3,33], or using the distributed transition-charge density derivative interaction proposed previously [34]. In these methods, the couplings of different vibrational modes were assumed to depend solely on the molecular structure. For the amide-I mode in peptides, if the two amide units are covalently bonded, the transition charge-based approaches have advantages over the transition dipole approach. However, as the inter unit distance increases, all the approaches tend to give the same answer.

The TDC is computed by using the following formula:

$$\beta_{ij} = \left[\left(\mu_i \cdot \mu_j\right) - 3\left(\mu_i \cdot e_{ij}\right)\left(\mu_j \cdot e_{ij}\right)\right] / r_{ij}^3, \tag{5}$$

where μ_i is the transition dipole in ($D\text{Å}^{-1}\text{amu}^{-1/2}$) units, r_{ij} is the distance between dipoles (in Å), e_{ij} is the unit vector connecting ith and jth vibrators.

The transition charge interaction approach has also been formulated for the amide-I mode in peptides [35]. In this method, atomic partial charge and transition charge are needed, which can be evaluated using the Mulliken charges and charge-fluxes via *ab initio* calculations [33,35-38]. The inter-site potential is approximated by the second-order expansion in terms of the normal modes [3]:

$$\beta_{ij} = \frac{1}{4\pi\varepsilon_0}\sum_{i,j} Q_i Q_j \left[\frac{1}{2}\sum_{a_i,b_j}\frac{\partial^2}{\partial Q_i \partial Q_j}\left(\frac{(q_{a_i}^0 + \delta q_{a_i} Q_i)(q_{b_j}^0 + \delta q_{b_j} Q_j)}{r_{a_i,b_j}}\right)\right]_{Q_i=Q_j=0}. \tag{6}$$

In equation (6), β_{ij} is the so-called pair-wise vibrational coupling for the ith and jth amide groups; a_i, b_j are the atoms that involved in the two amide-I normal mode displacement, which are C, O, N and H atoms here; $q_{a_i}^0$ is the atomic partial charge of the a_ith atom; δq_{a_i} is the transition charge for the a_ith atom in the normal mode Q_i; r_{a_i,b_j} is the distance between the two atoms; and ε_0 is the dielectric constant. We use a monopeptide model compound, namely *N*-methylacetamide (NMA), for parameterization, as also previously described [33,35]. Here, the charges and charge fluxes can be refined to produce the desired transition dipole strength for the amide-I band [37], or to fit IR and Raman signals [40,41]. For NMA, the charges and charge fluxes obtained at the B3LYP/6-31+G* level yields a transition dipole magnitude of 0.38 *D*, in fair agreement with a previous report [31]. Further, as pointed out earlier [3], other charges schemes, such as Merz-Kollman [42], CHELP [43], CHELPG [44], NPA [45] and dipole-derivative derived charges [39] are also potential choices for this purpose.

In the TDC approach, the angle between the transition dipole and amide C=O bond is usually set to between 15° and 23° to fit experimental IR spectra. In the TCI approach, the calculated orientation of the transition dipole is found to be ~ 20° with respect to the C=O bond axis and towards the nitrogen atom. This angle falls into the experimentally determined range (15 ° to 25°) for the model compound NMA [46]. However, various values of this angle have been obtained theoretically (between -19° and 20°) when using different force fields even for the same model compound [32,47-49].

When the through bond interaction is important, the *ab initio* computation approach has to be used. For peptides in conformation covering the entire Ramachandran space, vibrational coupling maps for the amide-I mode based *ab initio* computations have been documented in literature [38,50-52], A more detailed *ab initio* computation based coupling map for the amide-I mode is also available for peptides in helical conformations [3], or in the region of the polyproline-II conformations [53]. The local-mode frequency map for the amide-I modes of peptides has also been made available [51].

2.3. Potential energy distribution

To evaluate how much a normal mode is delocalized onto its neighboring unit of the same kind, the potential energy distribution (PED) analysis can be carried out on the basis of the internal coordinates. This method has been recognized for some time [32]. The obtained PED value can be used to describe the relative contributions of various displacement coordinates to the total change in potential energy during a specific vibrational motion. When a normal mode Q_k is excited, the potential energy V_k of the molecule can be expressed as [32]

$$V_k = \tfrac{1}{2} Q_k^2 \lambda_k , \tag{7}$$

where λ_k measures the potential energy change for unit displacement of Q_k, and

$$\lambda_k = \sum_{ij} F_{ij} L_{ik} L_{jk} . \tag{8}$$

Here F_{ij} is the force constant in internal coordinates, and L_{ik} is the element of the eigenvector of the GF matrix [23]. The PED values are obtained using the vibrational energy distribution analysis (VEDA) [54]. The information on the coordinate orientation, force constants in Cartesian coordinates and frequencies with atom displacement matrix are extracted from *ab initio* computations.

2.4. Simulation of 1D IR spectra

In the following, we introduce two simple frequency-domain methods for simulating 1D IR spectra of peptides. First, for the entire 3*N*-6 normal modes of a given molecule, a straightforward way of simulating its 1D IR spectra is to use the *ab initio* computed (anharmonic) frequencies and intensities. Assuming certain line broadening functions, one can obtain the

simulated broadband 1D IR spectra. A combination of Lorentzian and Gaussian functions is usually used for homogeneous and inhomogeneous contributions to the line broadening. Even though the widths of these two functions can be set flexibly for each vibration in order to compare with experimental IR spectra, the obtained line width is not physically meaningful.

The excitonic modeling, on the other hand, is particularly useful for simulating the linear IR spectra of a set of identical vibrational modes in the frequency domain. It has been used effectively to the amide-I mode of peptides. The excitonic band structure is illustrated in Figure 1, in which site states and excitonic states are shown. A set of coupled anharmonic oscillators, i.e., the site states $\{|m\rangle\}$, forms the one-quantum states $\{|k\rangle\}$. *The so-called one-exciton Hamiltonian for a particular polypeptide labeled by the index* n, *was chosen as* M *coupled harmonic oscillators* [3]*:*

$$H_n = \sum_m^M (\varepsilon + \xi_m^{(n)}) |m\rangle\langle m| + \sum_{m \neq l}^M \beta_{ml}^{(n)} |m\rangle\langle l| \tag{9}$$

In equation (9), ε is defined as the vibrational transition frequency (or site energy) of the mth amide-I mode (m=1 to M) in the nth polypeptide. The normal distribution (Gaussian distribution with the standard deviation σ) is very useful to describe the site energy fluctuations $\{\xi_m^{(n)}\}$ in the fashion of "white noise" (where n denotes sampling size). The ensemble properties can be obtained by averaging over N molecules. However, special distributions can also be employed to account for correlated energy fluctuations in the fashion of "color noise". The pair-wise coupling $\beta_{ml}^{(n)}$ can be computed using various coupling schemes described above. Standard bond lengths and angles can be generated easily for peptides with known coordinates of heavy atoms. Further, the diagonal disorder describes the static ensemble averaging, which is valid in the case of Bloch dynamics [55-57] where the fast and slow structural dynamics are separated in time.

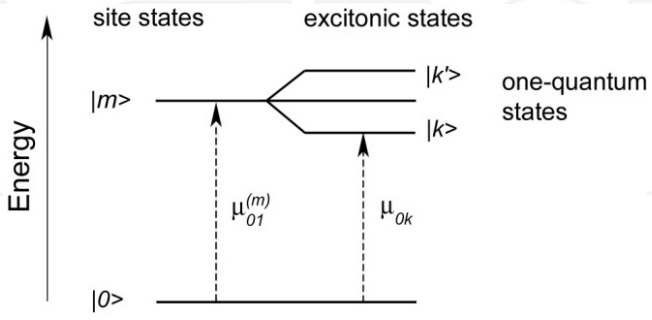

Figure 1. Excitonic model. A set of site states forms the one-excitonic band due to vibrational coupling. Only one-quantum states are given. Transition dipoles for both site states and excitonic states are shown.

The strength of the transition dipole of each eigenmode gives the total linear IR spectrum, as shown previously [3]:

$$S(\omega) = \left\langle \sum_{k}^{M} |\vec{\mu}_{0k}|^2 \left\{ \frac{\gamma_{k0}/\pi}{(\omega-\omega_{k0})^2+\gamma_{k0}^2} \right\} \right\rangle \tag{10}$$

where $\vec{\mu}_{0k} = \sum_{m=1}^{M} a_{km}^{(n)} \vec{\mu}_{01}^{(m)}$, $\vec{\mu}_{01}^{(m)}$ is the local transition dipole vector of the $v = 0 \rightarrow v = 1$ transition of the mth amide unit in a peptide conformation and $a_{km}^{(n)}$ is the amplitude of the site m in the eigenstate k. γ_{k0} is the homogeneous linewidth for the $|0\rangle \rightarrow |k\rangle$ transition.

3. Results and discussion

3.1. Conformation dependent amide-I normal mode vibration in peptide oligomers

First we examine the anharmonic parameters of the amide-I mode of a model dipeptide. The molecular structure of the glycine dipeptide (Ac-Gly-NMe, or $CH_3CONHC_\alpha H_2CONHCH_3$) is shown in Figure 2, in which backbone dihedral angles are defined to be ϕ ($CNC_\alpha C$) and ψ ($NC_\alpha CN$). Here ten well-known secondary conformations are chosen, namely α_{L2}-helix (ϕ = +90°, ψ = -90°); π-helix (-57°, -70°); polyproline-II (PP_{II}, -75°, +135°); α_{L1}-helix (+60°, +60°); C_7 conformation (+82°, -69°); extended structure (180°, -180°); α-helix (-58°, -47°); 3_{10}-helix (-50°, -25°); anti-parallel β-sheet (-139°, +135°); and parallel β-sheet (-119°, +113°). Harmonic and anharmonic frequencies of the two amide-I modes in these dipeptides are evaluated using the density functional theory and Hartree-Fock (HF) methods. The results from the two methods are found to be highly correlated, as shown in Figure 3. Two amide-I normal modes in these dipeptides are linear combinations of the two amide-I local modes, which are dominated by the C=O stretching vibration. In the left column of Figure 3, two amide-I normal mode frequencies (harmonic picture) are shown: one is the symmetric stretching and has a relatively higher frequency (panel A) and the other is the asymmetric stretching whose frequency is lower (panel C). In order to better compare the HF frequencies (squares) and DFT frequencies (circles), the HF results are subtracted by 150 cm^{-1}. The results show that the calculated normal-mode harmonic frequencies at the level of Hartree-Fock theory have the same trend as those obtained at the level of the density functional theory. One can also draw the same conclusion from the anharmonic frequencies that are given in the right column of Figure 3 (panel B and D). In addition, the frequency difference between the high- and low-frequency modes in the harmonic picture (panel E) and in the anharmonic picture (panel F) are also meaningful to compare, because the frequency separation is closely related to the inter-mode coupling. Clearly the frequency separations obtained by the HF and DFT methods are also in good agreement, for both the harmonic and anharmonic cases. Further more, for the ten conformations the averaged DFT anharmonic frequency of the high-frequency mode is found to be 31.7 cm^{-1} lower than that of the harmonic frequency, indicating the effect of considering the

http://dx.doi.org/10.5772/58888

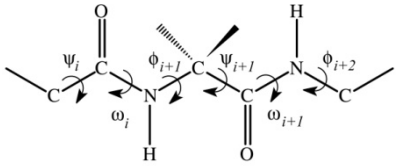

Figure 2. A fragment of peptide oligomer showing dihedral angles for peptide back bone and amide unit. The middle carbon is C_α.

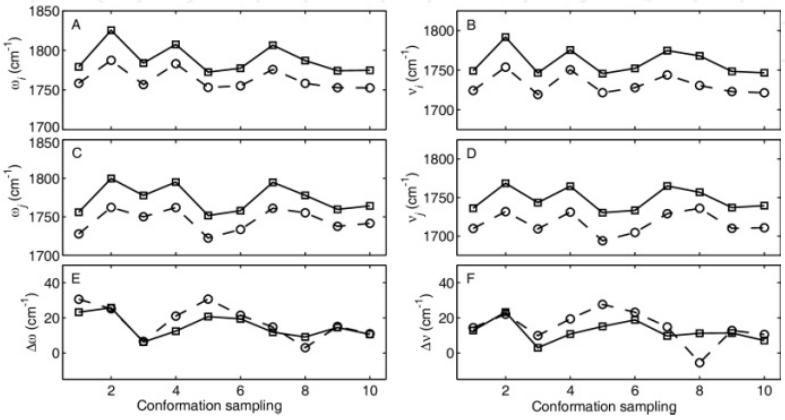

Figure 3. Harmonic and anharmonic frequencies and their difference (in cm^{-1}) of the two amide-I modes in ten representative peptide conformations obtained at the level of DFT (circle) and HF (square) for comparison. 1: α_{L2}-helix (+90°, -90°); 2: π-helix (-57°, -70°); 3: PP_{II} (-75°, +135°); 4: α_{L1}-helix (+60°, +60°); 5: C_7 (+82°, -69°); 6: extended structure (+180°, -180°); 7: α-helix (-58°, -47°); 8: 3_{10}-helix (-50°, -25°); 9: anti-parallel β-sheet (-139°, +135°); and 10: parallel β-sheet (-119°, +113°). Panel A: harmonic frequency for the high-frequency mode; panel B: anharmonic frequency for the high-frequency mode; panel C: harmonic frequency for the low-frequency mode; panel D: anharmonic frequency for the low-frequency mode; panel E: harmonic frequency difference; and panel F: anharmonic frequency difference. The HF results are subtracted by 150 cm^{-1}. Adapted from reference [30] with permission.

anharmonic potential. Similarly, the lowered value is 28.7 cm^{-1} for the low-frequency mode. On the other hand, for the HF results, the anharmonic frequency drops 29.0 cm^{-1} for the high-frequency mode, and 26.0 cm^{-1} for the low-frequency mode. This indicates a similar anharmonic energy decrease using the two different methods. However, it is also noted that for some typical structures the frequency splitting show method-dependence, which will result in method-dependent inter-mode coupling, as discussed below. The performance of the DFT (B3LYP) and HF methods in computing the anharmonicities of the amide-I modes of peptide oligomers has been examined previously [29] and it was shown that the two methods were able to provide an optimum compromise between reliability and computer time.

Next, the full conformation space ($-180° \le \phi \le +180°$, $-180° \le \psi \le +180°$) for peptide backbone is explored with total 169 samplings of partially optimized structures ($\Delta\phi = \Delta\psi = 30°$). The partial optimization is performed at the HF level of theory by fixing ϕ and ψ to desired values each

time, to sample the entire conformational space. The result is given in Figure 4. The two amide-I normal-mode frequencies (panel A and B) show significant conformation sensitivity, with different dependences on the two dihedral angles. In panel A, the harmonic high-frequency component exhibits a low-frequency region that is anti-diagonally arranged (from lower right to upper left). In panel B, the harmonic low-frequency component, however, exhibits a similarly arranged low-frequency region, but in much smaller area. The conformational dependences of the anharmonic normal-mode frequencies, which are given in panel C and D respectively, resemble those of their harmonic counterparts (panel A and B respectively). However, a detailed analysis shows subtle difference in mean value and distribution of the harmonic and anharmonic frequencies: on average the anharmonic frequency drops *ca*. 30 cm^{-1} from the harmonic frequency. Further, the obtained harmonic frequencies change more dramatically along ψ in the region of ($-90° \le \phi \le 90°$), as shown in Figure 4 (panel A and B). A similar behavior has been observed in a previous study [52]. Our results show that such a pattern still remains in the behavior of the anharmonic frequencies ν_i and ν_j in the (ψ, ϕ) conformational space (panel C and D).

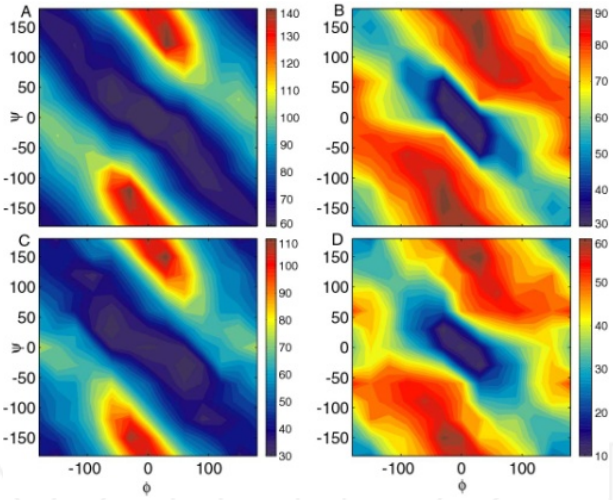

Figure 4. Conformation-dependent normal-mode frequencies (in cm^{-1}) for the two amide-I modes with and without anharmonic correction. (A): high-frequency harmonic component (ω_i); (B): low-frequency harmonic component (ω_j); (C): high-frequency anharmonic component (ν_i); and (D): low-frequency anharmonic component (ν_j). Frequencies are subtracted by 1900 cm^{-1}. Adapted from reference [30] with permission.

3.2. Conformation dependent amide-I local mode vibration in peptide oligomers

Local-mode frequencies can be obtained by decoupling the two amide-I normal modes in either the harmonic or anharmonic picture. The results are shown in Figure 5. In the harmonic picture, the obtained zero-order amide-I vibration frequency (denoted as ω_i^0) of the NMe side (or the C-terminus side, as shown in Figure 2) is generally higher than the zero-order frequency

http://dx.doi.org/10.5772/58888

(denoted as ω_j^0) of the Ac side (or the N-terminus side). The two harmonic local-mode frequencies also show quite different dihedral-angle dependences, which is clearly shown in A and B panels. Figure 5A depicts a relatively larger low-frequency area (anti-diagonally located) for ω_i^0, with a mean value of $\bar{\omega}_i^0$ =1943.8 cm^{-1}. Figure 5B shows a relatively smaller low-frequency area with a mean value of $\bar{\omega}_j^0$ =1934.3 cm^{-1}. Further, the conformational dependence of the harmonic local-mode frequencies bears a strong resemblance to that of the normal-mode frequencies. This is evident by comparing Figure 5 and Figure 4. The harmonic local-mode picture shown in Figure 5 A and B is also quite similar to that reported in a previous work [58], in which B3LYP functional and 6-31+G* basis set were used.

In the anharmonic picture, the conformational dependence of the local-mode frequencies differs slightly from that in the harmonic picture. The results are shown in Figure 5, C and D panels. In panel C, the conformational dependence of the zero-order vibrational frequency (ν_i^0) of the amide-I unit at the C-terminus side is shown, while in panel D the conformational dependence of the zero-order vibrational frequency (ν_j^0) of the amide-I unit at the N-terminus side is shown. It is found that their mean values are $\tilde{\nu}_i^0$ = 1914.3 cm^{-1} and $\tilde{\nu}_j^0$ = 1904.5 cm^{-1} respectively, thus $\tilde{\nu}_i - \tilde{\nu}_i^0$ = 5.5 cm^{-1} and $\tilde{\nu}_j - \tilde{\nu}_j^0$ = -5.1 cm^{-1}. This means that in the anharmonic picture, the average frequency splitting between the two amide-I modes due to coupling is 10.6 cm^{-1}, while in the harmonic picture the average frequency splitting is slightly larger (12.0 cm^{-1}). One can also estimate the average frequency splitting $\left(\tilde{\nu}_i^0 - \tilde{\nu}_j^0\right)$, which is 9.8 cm^{-1}, indicating the extend of local-mode non-degeneracy in the anharmonic picture.

Thus the computation results shown in Figure 5 indicate a generally non-degenerate zero-order frequency picture under both the harmonic and anharmonic approximations. Such a non-degeneracy is believed to be an intrinsic property of polypeptides. For example, in a ^{13}C labeled β-hairpin two amide-I modes on the same peptide chain are found to have different zero-order frequencies by both 1D and 2D IR studies [59]. The non-degeneracy of the local states is believed to be due to the variation of local chemical and solvent environment of peptide amide group (-CONH-) [60]. Such a non-degenerate local-mode picture should be taken into account during empirical modeling of the 1D and 2D IR spectra of peptides and proteins. In particular, a set of zero-order transition energies can be initialized as the diagonal elements of the one-exciton Hamiltonian. Because these local-mode frequencies are backbone dihedrals (ϕ, ψ) dependent, they bear site-specific local structure characteristics and are also sensitive to solvent environment. On the other hand, the normal modes in peptides do not carry direct local-structure identities because of the mode delocalization. Under such circumstances the IR frequency and peptide structure relationship cannot be established in a straightforward way. It is for these reasons that peak assignment in conventional IR spectroscopy could be troublesome.

Further, because the amide-I local-mode frequency in the conformational space in the anharmonic picture appears to be quite similar to that in the harmonic picture one may scale the frequency from the latter to the former. This suggests a simple way to approximately obtain the anharmonic frequencies. However, care should be taken when the scaling method is

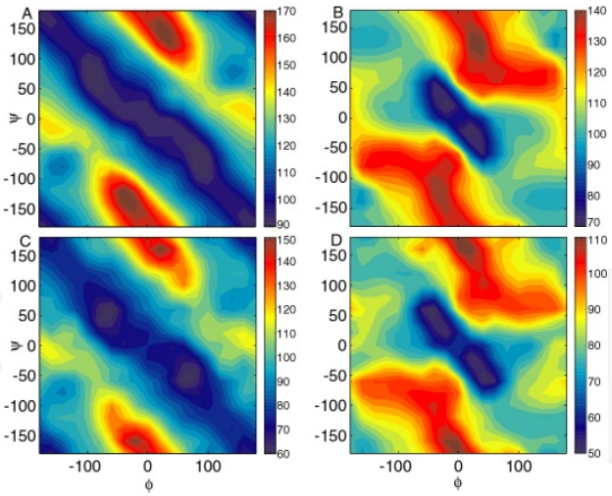

Figure 5. Conformation-dependent local-mode frequencies (in cm^{-1}) for the two amide-I modes with and without anharmonic correction. (A): high-frequency harmonic component (ω_i^0); (B): low-frequency harmonic component (ω_j^0); (C): high-frequency anharmonic component (ν_i^0); and (D): low-frequency anharmonic component (ν_j^0). Frequencies were subtracted by 1900 cm^{-1}. Adapted from reference [30] with permission.

utilized, because it is well known that the frequency scaling is not applicable simultaneously to all the 3*N*-6 modes in a molecule. The frequency scaling scheme would be useful only when a very limited number of modes were considered; for example, amide-I modes only in this case. Furthermore, to obtain solution-phase vibrational frequencies, solution-phase frequency models has to be established, and several of such have become available particularly for the amide-I modes [58,61,62]. In addition, for a solvated peptide, the solvation effect may be added to the scaled harmonic frequencies or to the un-scaled anharmonic frequencies so as to yield modified zero-order frequencies for spectral modeling.

3.3. Anharmonicity, coupling and mode delocalization

In this work the diagonal anharmonicity is defined as the decrease of the energy gap between the first excited state and its overtone state ($n = 1$ and $n = 2$ where n is the vibrational quantum number) with respect to that of the ground state and first excited state ($n = 0$ and $n = 1$). The diagonal anharmonicity, inter-mode coupling, and mode delocalization are very important anharmonic parameters. The conformational dependence of these parameters is examined and the results are given in Table 1 for several dipeptides in which two units are either covalently bonded or hydrogen bonded.

We first discuss the anharmonicity of a single vibrator case. In an isolated peptide unit, for example, *trans*-NMA, the amide-I mode is highly localized, the diagonal anharmonicity is found to be 18.0 cm^{-1} by computation. The diagonal anharmonicity begins to change and exhibits conformational sensitivity in a two-vibrator case. For example in alanine dipeptide

http://dx.doi.org/10.5772/58888

with the α-helical conformation (–58°, –47°) the anharmonicities of both amide-I modes are smaller than that in the isolated amide unit, whereas in the conformation (–75°, +135°) and both anharmonicities are comparable with the value in the isolated amide unit. In AcProNMe the anharmonicity decreases for the C=O hydrogen-bonded amide-I mode. In hydrogen-bonded *trans*-NMA dimer, for the free and C=O hydrogen-bonded amide-I modes, the two diagonal anharmonicities decrease even more. Experimentally, an anharmonicity of 16.0 cm^{-1} was reported for NMA [63], and smaller values were reported for two spatially connected amide units in different conformations, for example, 9-11 cm^{-1} in the α-helix [64] and 13±2 cm^{-1} in the amino-end amide of $AcProNH_2$ [65]. Also, relatively large value (*ca.*16.0 cm^{-1}) was found for two amide units in an alanine dipeptide with a negligible coupling constant [53]. Thus the calculated values correlate reasonably with the experimental results. This suggests that the diagonal anharmonicity of the amide-I mode may serve as a probe for the secondary structure of peptides, while only the off-diagonal anharmonicity was believed to be useful previously for structural determination because of its link to the pair-wise coupling of two vibrators.

As shown in equation (4), the wave function mixing angle is determined by the coupling and transition energy gap of two local modes. Large mixing angle means large mode delocalization. The results of the mixing angle and inter-mode coupling for several dipeptides are listed in Table 1. For alanine dipeptide in the α-helical conformation (ϕ, = –58°, ψ = –47°), the mixing angle between two local states is ξ = 31.8°, while the inter-mode coupling is 4.9 cm^{-1} in the anharmonic picture (or 6.0 cm^{-1} in the harmonic picture). Thus somewhat different coupling is expected when using the anharmonic frequency scheme rather than the harmonic case, even though the latter approach has been very popular previously [3,38,66]. For the dipeptide with dihedral angles of (–75°, +135°), the mixing angle is $\xi \approx 0.1°$, and the coupling is very small (between –0.01 and –0.08 cm^{-1}) regardless of which frequency scheme is used. For the dipeptide with dihedral angles of (–50°, –25°), the mixing angle is ξ = 69.5° and the inter-mode coupling is 6.0 cm^{-1} in the anharmonic picture (but –1.0 cm^{-1} in the harmonic picture). For AcProNMe, the mixing angle is ξ = 8.9° and the coupling is *ca.* –8.2 cm^{-1} using either frequency scheme. In the case of the *trans*-NMA dimer, the mixing angle between two local states is ξ = 24.2°, while the inter-mode coupling is –3.1 cm^{-1} in the anharmonic picture or –5.0 cm^{-1} in the harmonic picture. Further, from the results shown in Table 1, one sees that generally the larger the diagonal anharmonicity, the smaller the mixing angle. The correlation between the anharmonicity and mode delocalization has been noted previously in the case of the C=O stretching modes of acetic acid dimer [67].

The term $|\tan 2\xi|$ is a very sensitive measure of the vibrational delocalization. However, from equation (4) one obtains $|\tan 2\xi| = \left|\beta_{ij}/\left(\nu_i^0 - \nu_j^0\right)\right|$, suggesting that highly delocalized states may not be strongly coupled. This is because, $|\tan 2\xi|$ is determined by the ratio of the coupling and frequency separation. Thus for the case of a significant coupling but a much larger energy separation, one could still have $|\tan 2\xi| \ll 1$, i.e., localized but still strongly coupled states. Two typical examples are shown in Table 1. For alanine dipeptide in the α-helical conformation, the two amide-I modes are both significantly delocalized ($|\tan 2\xi| = 1.0$) and coupled (β_{ij} = 4.9 cm^{-1}). For the remaindering dipeptides, the amide-I modes are largely

localized (with small $|\tan 2\xi|$), but the strength of coupling varies. In particular, proline dipeptide AcProNMe shows a significant coupling (β_{ij} = -8.2 cm^{-1}), but the two states are pretty much localized, which is mainly because of the presence of two largely separated transition frequencies.

Further, the degree of mode delocalization can be characterized by using the potential energy distribution that describes the relative contributions of various displacement coordinates to the total change in potential energy during the vibration. Here we examine the mode delocalization in gas-phase and in explicit solvent environment. We carry out computations at the harmonic level for alanine dipeptide systems in either α-helical or β-sheet conformation, with four water molecules included in each case. The results are given below (Figure 6 and Table 2). Similar short peptide systems were examined previously to study the hydration effect of peptides [68]. The solution-phase local-mode frequencies are found to red shift from those in the gas-phase because the two amide units are both H-bonded with solvent molecules (Table 2). However, it is clear the frequency separations between the high-frequency mode and low-frequency mode for ADP in gas and in solution phases are quite similar. So it is expected that the decoupled local mode frequency separations are similar too. In other words, solvent effect on frequency separation (and mode localization caused by that) is not significantly affected by the first hydration layer in this case.

ith and jth amide-I modes	alanine dipeptide			proline dipeptide	NMA dimer
(ϕ, ψ)	(–58, –47)	(–75, +135)	(–50, –25)	(–83, +71)	
ν_i^0	1734.2	1714.0	1734.8	1711.4	1704.2
ν_j^0	1729.3	1675.0	1748.7	1660.5	1698.6
Δ_{ii}	11.5	21.3	14.9	19.9	8.7
Δ_{jj}	11.7	19.3	21.9	17.3	13.3
β_{ij}	4.9	–0.1	6.0	–8.2	–3.1
ξ	31.8	0.1	69.5	8.9	24.2
$\lvert\beta_{ij}/(\nu_i^0-\nu_j^0)\rvert$	1.0	2.5×10^{-3}	0.4	0.2	0.6

Table 1. Anharmonic local-mode frequency (ν, in cm^{-1}), anharmonicity (Δ, in cm^{-1}), coupling (β, in cm^{-1}), and wave function mixing angle (ξ, in degree) for two nearest neighboring amide units in various dihedral angles (ϕ and ψ, in degree). The diagonal anharmonicity is obtained from the *ab initio* calculations. Adapted from reference [29] with permission

One sees that the PED values of the two modes decrease similarly (with a few percent variation). This is found to be the case for both conformations. Here the decreased PED indicates more mode delocalization, reaching over water bending modes through hydrogen-bonding interactions. This hydration picture is reasonable for short peptides because one can hardly have one amide unit hydrogen-bonded with solvent and another not, in a solvated short

http://dx.doi.org/10.5772/58888

peptide. This suggests that given a homogeneous solvent environment, the amide-I mode-delocalization in short peptide would probably change similarly for each amide unit. Note that for longer peptides containing different side chains and forming intramolecular hydrogen-bonds, it might be true that only some of the amide-I frequencies would be red-shifted due to hydrogen-bonding interaction, but certainly this is a case-dependent story.

mode	α-helix				β-sheet			
	gas phase		solution phase		gas phase		solution phase	
	ω_i	PED	ω_i	PED	ω_i	PED	ω_i	PED
a	1771.1	0.57	1733.7	0.53	1749.4	0.56	1716.3	0.36
b	1758.0	0.58	1721.7	0.46	1733.3	0.60	1694.0	0.41

Table 2. Computed harmonic frequency and PED for the amide-I modes in ADP- $(H_2O)_4$ in the α-helix and β-sheet conformations at the level of B3LYP/6-31+G*.

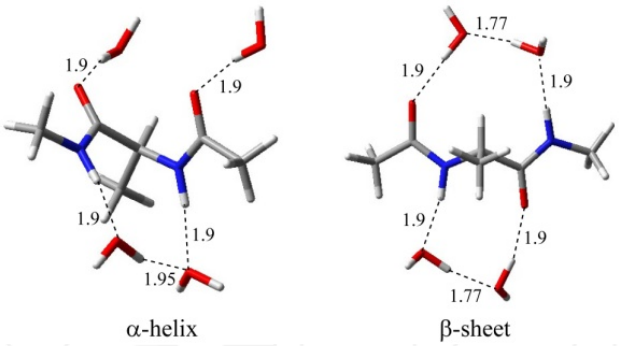

Figure 6. Optimized ADP- $(H_2O)_4$ systems in the α-helix (left) and β-sheet (right) conformations at the level of B3LYP/6-31+G*. Distance is in Å.

3.4. Simulated 1D IR spectra of peptides

The simulated 1D IR spectra of two typical turn conformations (Table 3) employing the vibrational exciton model in the frequency domain are shown in Figure 7. More details can be found in a recent work [3]. Discernable conformational-dependent spectral features are seen in simulated 1D IR spectra of these peptide structures. The spectral features include absorption peak positions and line width profiles. For the γ–turn, two amide-I local modes are coupled

and transition intensities are not equal. For the β–turn, three coupled local transitions form excitonic band structure (normal modes) that differs from that of the γ–turn. In Figure 7, stick spectrum are also given in each panel. Inhomogeneous distribution of the transition energies are clearly shown in each case [69]. Further, because of transition intensity transfer, a direct result of vibrational coupling, the computed 1D IR spectra show patterns that significantly different from the local-mode picture with three independent bands.

species	dihedral angles [a]							hydrogen-bonding ring
γ–turn	ω_1	ϕ_2	ψ_2	ω_2				
classic	+172.6	74.9	-75.0	−170.8				C_7
β–turn	ω_1	ϕ_2	ψ_2	ω_2	ϕ_3	ψ_3	ω_3	
type I	+175.3	−60.0	−30.0	−177.1	−90.0	+0.0	−171.2	C_{10}

[a]. Defined in Figure 2.

Table 3. Glycine-based peptide oligomers in turn conformations: Ac–Gly_n–NMe (n = 1 for the γ–turn and n = 2 for the β–turn).

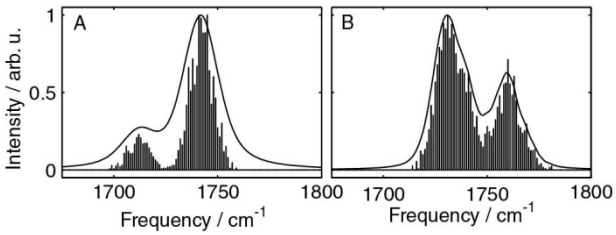

Figure 7. Simulated 1D IR of selected peptide fragments in (A) the classic γ-turn and (B) the type-I β-turn. Sticks indicate ensemble sampling.

4. Conclusions

This chapter discusses the methods and application of anharmonic vibration parameters for the purpose of connecting the secondary structure of proteins and peptides to their IR spectra. Using the amide-I mode in particular, the usefulness of the methods is clearly demonstrated. The performance of the DFT and HF theories in predicting the anharmonic frequencies are compared and the conformational dependence of the obtained parameters are examined. The methods to compute vibrational coupling are also reviewed and examples are discussed. The coupled nature of the amide-I band for typical secondary structures is analyzed using the potential energy distribution function, and the local-mode properties (frequency and coupling) are discussed. Since the solvent effect on these parameters is unavoidable, as has shown for PED analysis, solvent molecules must be taken into account in assessing the vibrational

properties of solute. Polarizable continuum method [70] for solvent model can be used for such purposes. In addition, site-dependent dynamical interactions between peptide and water molecules in the hydration shells needs to be examined by molecular dynamics simulations employing proper molecular mechanical force fields, so that the statistical distributions and correlations of the transition frequencies can be computed. This can be done by carrying our instantaneous normal mode analysis, for example. Time-dependent vibrational couplings can also be computed based on the molecular dynamics trajectories. Nevertheless, simultaneous assessment of vibrational parameters of multiple vibrational modes shall prove useful in understanding the characteristics of linear and nonlinear infrared spectra of both static and equilibrium dynamical structures of proteins, peptides and other biomolecules [71].

Acknowledgements

I would like to thank my students in the Quantum Multidimensional Infrared Spectroscopy group in the Molecular Reaction Laboratory of the Institute of Chemistry, for their contributions to this work.

This work was supported by the National Natural Science Foundation of China (20773136, 30870591 and 21173231), and by the Chinese Academy of Sciences (Hundred Talent Fund).

Author details

Jianping Wang*

Address all correspondence to: jwang@iccas.ac.cn

Institute of Chemistry, the Chinese Academy of Sciences, Beijing National Laboratory for Molecular Sciences, Beijing, P. R. China.

References

[1] Mantsch HH, Chapman D. Infrared spectroscopy of biomolecules, Wiley-Liss, New York, 1996.

[2] Barth A, Zscherp C. What vibrations tell us about proteins. Quarterly Reviews of Biophysics 2002;35:369-430.

[3] Wang J, Hochstrasser RM. Characteristics of the two-dimensional infrared spectroscopy of helices from approximate simulations and analytic models. Chemical Physics 2004;297:195-219.

[4] Miyazawa T. Perturbation treatment of the characteristic vibrations of polypeptide chains in various configurations. The Journal of Chemical Physics 1960;32:1647-52.

[5] Miyazawa T, Blout ER. The infrared spectra of polypeptides in various conformations: amide I and II bands. Journal of the American Chemical Society 1961;83:712-19.

[6] Chirgadze YN, Nevskaya NA. Infrared spectra and resonance interaction of amide-I vibration of the antiparallel-chain pleated sheet. Biopolymers 1976;15:607-25.

[7] Mukherjee S, Chowdhury P, Gai F. Effect of dehydration on the aggregation kinetics of two amyloid peptides. The Journal of Physical Chemistry B 2008;113:531-35.

[8] Cerf E, Sarroukh R, Tamamizu-Kato S, Breydo L, Derclaye S, Dufrêne YF, Narayanaswami V, Goormaghtigh E, Ruysschaert JM, Raussens V. Antiparallel β-sheet: a signature structure of the oligomeric amyloid β-peptide. Biochemical Journal 2009;421:415-23.

[9] Goormaghtigh E, Cabiaux V, Ruysschaert JM. Determination of soluble and membrane protein structure by Fourier transform infrared spectroscopy. I. Assignments and model compounds. Subcellular Biochemistry 1994;23:329-62.

[10] Watson TM, Hirst JD. Density functional theory vibrational frequencies of amides and amide dimers. The Journal of Physical Chemistry A 2002;106:7858-67.

[11] Merrick JP, Moran D, Radom L. An evaluation of harmonic vibrational frequency scale factors. The Journal of Physical Chemistry A 2007;111:11683-700.

[12] Cowan ML, Bruner BD, Huse N, Dwyer JR, Chugh B, Nibbering ETJ, Elsaesser T, Miller RJD. Ultrafast memory loss and energy redistribution in the hydrogen bond network of liquid H2O. Nature 2005;434:199-202.

[13] Asbury JB, Steinel T, Stromberg C, Corcelli SA, Lawrence CP, Skinner JL, Fayer MD. Water dynamics: vibrational echo correlation spectroscopy and comparison to molecular dynamics simulations. The Journal of Physical Chemistry A 2004;108:1107-19.

[14] Lee K-K, Park K-H, Park S, Jeon S-J, Cho M. Polarization-angle-scanning 2D IR spectroscopy of coupled anharmonic oscillators: A polarization null angle method. The Journal of Physical Chemistry B 2011;115:5456-64.

[15] King JT, Kubarych KJ. Site-specific coupling of hydration water and protein flexibility studied in solution with ultrafast 2D-IR spectroscopy. Journal of the American Chemical Society 2012;134:18705-12.

[16] Li D, Yang F, Han C, Zhao J, Wang J. Correlated high-frequency molecular motions in neat liquid probed with ultrafast overtone two-dimensional infrared spectroscopy. The Journal of Physical Chemistry Letters 2012;3:3665-70.

[17] Yu P, Yang F, Zhao J, Wang J. Hydration dynamics of cyanoferrate anions examined by ultrafast infrared spectroscopy. The Journal of Physical Chemistry B 2014;118:3104-14.

[18] Hochstrasser RM. Two-dimensional spectroscopy at infrared and optical frequencies. Proceedings of the National Academy of Sciences of the United States of America 2007;104:14190-96.

[19] Maekawa H, Ballano G, Toniolo C, Ge N-H. Linear and two-dimensional infrared spectroscopic study of the amide I and II modes in fully extended peptide chains. The Journal of Physical Chemistry B 2010;115:5168-82.

[20] Middleton CT, Marek P, Cao P, Chiu C-c, Singh S, Woys AM, de Pablo JJ, Raleigh DP, Zanni MT. Two-dimensional infrared spectroscopy reveals the complex behaviour of an amyloid fibril inhibitor. Nature Chemistry 2012;4:355-60.

[21] Costard R, Heisler I, A., Elsaesser T. Structural dynamics of hydrated phospholipid surfaces probed by ultrafast 2D spectroscopy of phosphate vibrations. The Journal of Physical Chemistry Letters 2014;5:506-11.

[22] Nielsen HH. The vibration-rotation energies of molecules. Reviews of Modern Physics 1951;23:90-136.

[23] Califano S: Vibrational states, John Wiley and Sons, London, New York, Sydney, Toronto, 1976.

[24] Barone V. Anharmonic vibrational properties by a fully automated second-order perturbative approach. The Journal of Chemical Physics 2005;122:014108/1-08/10.

[25] Barone V. Accurate vibrational spectra of large molecules by density functional computations beyond the harmonic approximation: The case of azabenzenes. The Journal of Physical Chemistry A 2004;108:4146-50.

[26] Zhao J, Wang J. Chain-length and mode-delocalization dependent amide-I anharmonicity in peptide oligomers. The Journal of Chemical Physics 2012;136:214112.

[27] Wang J. Conformational dependence of anharmonic NH stretch vibration in peptides. Chemical Physics Letters 2009;467:375-80.

[28] Zheng ML, Zheng DC, Wang J. Non-native side chain IR probe in peptides: Ab initio computation and 1D and 2D IR spectral simulation. The Journal of Physical Chemistry B 2010;114:2327-36.

[29] Wang J, Hochstrasser RM. Anharmonicity of Amide Modes. The Journal of Physical Chemistry B 2006;110:3798-807.

[30] Wang J. Conformational dependence of anharmonic vibrations in peptides: amide-I modes in model dipeptide. The Journal of Physical Chemistry B 2008;112:4790-800.

[31] Cheam TC, Krimm S. Transition dipole interaction in polypeptides: ab initio calculation of transition dipole parameters. Chemical Physics Letters 1984;107:613-16.

[32] Krimm S, Bandekar J. Vibrational spectroscopy and conformation of peptides, polypeptides, and proteins. Advances in Protein Chemistry 1986;38:181-364.

[33] Hamm P, Lim M, DeGrado WF, Hochstrasser RM. The two-dimensional IR nonlinear spectroscopy of a cyclic penta-peptide in relation to its three-dimensional structure. Proceedings of the National Academy of Sciences of the United States of America 1999;96:2036-41.

[34] Moran A, Mukamel S. The origin of vibrational mode couplings in various secondary structural motifs of polypeptides. Proceedings of the National Academy of Sciences of the United States of America 2004;101:506-10.

[35] Hamm P, Hochstrasser RM, in M.D. Fayer (Ed.), Ultrafast Infrared and Raman Spectroscopy. Marcel Dekker Inc., New York, 2001, p. 273-347.

[36] Dybal J, Cheam TC, Krimm S. Carbonyl stretch mode splitting in the formic acid dimer: electrostatic models of the intermonomer interaction. Journal of Molecular Structure 1987;159:183-94.

[37] Torii H, Tasumi M. Infrared intensitites of vibrational modes of an -a-helical polypeptide: calculations based on the equilibrium charge/charge flux (ECCF) model. Journal of Molecular Structure 1993;300:171-79.

[38] Hamm P, Woutersen S. Coupling of the amide I modes of the glycine dipeptide. Bulletin of the Chemical Society of Japan 2002;75:985-88.

[39] Qian W, Krimm S. Origin of the C=O stretch mode splitting in the formic acid dimer. The Journal of Physical Chemistry 1996;100:14602-08.

[40] Yokoyama I, Miwa Y, Machida K. Extended molecular mechanics calculations of thermodynamic quantities, structures, vibrational frequencies, and infrared absorption intensities of formic acid monomer and dimer. Journal of the American Chemical Society 1991;113:6458-64.

[41] Yokoyama I, Miwa Y, Machida K. Simulation of Raman spectra of formic acid monomer and dimer in the gaseous state by an extended molecular mechanics method. The Journal of Physical Chemistry 1991;95:9740-46.

[42] Besler BH, Merz KMJ, Kollman PA. Atomic charges derived from semiempirical methods. Journal of Computational Chemistry 1990;11:431-39.

[43] Chirlian LE, Francl MM. Atomic charges derived from electrostatic potentials: A detailed study. Journal of Computational Chemistry 1987;8:894-905.

[44] Breneman CM, Wiberg KB. Determining atom-centered monopoles from molecular electrostatic potentials. The need for high sampling density in formamide conformational analysis. Journal of Computational Chemistry 1990;11:361-73.

[45] Reed AE, Weinstock RB, Weinhold F. Natural population analysis. The Journal of Chemical Physics 1985;83:735-46.

[46] Bradbury EM, Elliott A. The infrared spectrum of crystalline N-methylacetamide. Spectrochimica Acta 1963;19:995-1012.

[47] Torii H, Tasumi M. Model calculations on the amide-I infrared bands of globular proteins. The Journal of Chemical Physics 1992;96:3379-87.

[48] Dwivedi AM, Krimm S. Vibrational analysis of peptides, polypeptides, and proteins. X. Poly(glycine I) and its isotopic derivatives. Macromolecules 1982;15:177-85.

[49] Rey-Lafon M, Forel MT, Garrigou-Lagrange C. Study of normal modes of cis- and trans-amide groups using force fields of d-valarolactam and N-methylacetamide. Spectrochimica Acta, Part A 1973;29:471-86.

[50] Torii H, Tasumi M. Ab initio molecular orbital study of the amide I vibrational interactions between the peptide groups in di- and tripeptides and considerations of the conformation of the extended helix. Journal of Raman Spectroscopy 1998;29:81-86.

[51] la Cour Jansen T, Dijkstra AG, Watson TM, Hirst JD, Knoester J. Modeling the amide I bands of small peptides. The Journal of Chemical Physics 2006;125:044312/1.

[52] Gorbunov RD, Kosov DS, Stock G. Ab initio-based exciton model of amide I vibrations in peptides: Definition, conformational dependence, and transferability. The Journal of Chemical Physics 2005;122:224904-12.

[53] Kim YS, Wang J, Hochstrasser RM. Two-dimensional infrared spectroscopy of the alanine dipeptide in aqueous solution. The Journal of Physical Chemistry B 2005;109:7511-21.

[54] Jamróz MH. Vibrational energy distribution analysis VEDA 4, Warsaw, 2004.

[55] Mukamel S: Principles of nonlinear optical spectroscopy, Oxford University Press, 1995.

[56] Cho M: Two-dimensional optical spectroscopy, CRC Press, Boca Raton, London, New York, 2009.

[57] Hamm P, Zanni M: Concept and methods of 2D infrared spectroscopy, Cambridge University Press, Cambridge, New York, Melbourne, Madrid, Cape Town, Singapore, Sao Paulo, Delhi, Tokyo, Mexico City, 2011.

[58] Jansen TL, Knoester J. A transferable electrostatic map for solvation effects on amide I vibrations and its application to linear and two-dimensional spectroscopy. The Journal of Chemical Physics 2006;124:044502/1-02/11.

[59] Wang J, Chen J, Hochstrasser RM. Local structure of β-hairpin Isotopomers by FTIR, 2D IR, and ab initio theory. The Journal of Physical Chemistry B 2006;110:7545-55.

[60] Wang J, Zhuang W, Mukamel S, Hochstrasser RM. Two-dimensional infrared spectroscopy as a probe of the solvent electrostatic field for a twelve residue peptide. The Journal of Physical Chemistry B 2008;112:5930-37.

[61] Schmidt JR, Corcelli SA, Skinner JL. Ultrafast vibrational spectroscopy of water and aqueous N-methylacetamide: comparison of different electronic structure/molecular dynamics approaches. The Journal of Chemical Physics 2004;121:8887-96.

[62] Hayashi T, Zhuang W, Mukamel S. Electrostatic DFT map for the complete vibrational amide band of NMA. The Journal of Physical Chemistry A 2005;109:9747-59.

[63] Hamm P, Lim M, Hochstrasser RM. Structure of the amide I band of peptides measured by femtosecond nonlinear-infrared spectroscopy. The Journal of Physical Chemistry B 1998;102:6123-38.

[64] Fang C, Wang J, Kim YS, Charnley AK, Barber-Armstrong W, Smith AB, III, Decatur SM, Hochstrasser RM. Two-dimensional infrared spectroscopy of isotopomers of an alanine rich alpha-helix. The Journal of Physical Chemistry B 2004;108:10415-27.

[65] Rubtsov IV, Hochstrasser RM. Vibrational dynamics, mode coupling and structure constraints for acetylproline-NH2. The Journal of Physical Chemistry B 2002;106:9165-71.

[66] Ham S, Cha S, Choi J-H, Cho M. Amide I modes of tripeptides: Hessian matrix reconstruction and isotope effects The Journal of Chemical Physics 2003;119:1451-61.

[67] Lim M, Hochstrasser RM. Unusual vibrational dynamics of the acetic acid dimer. The Journal of Chemical Physics 2001;115:7629-43.

[68] Bohr HG, Frimand K, Jalkanen KJ, Nieminen RM, Suhai S. Neural-network analysis of the vibrational spectra of N-acetyl L-alanyl N8-methyl amide conformational states. Physical Review E 2001;64:021905-1.

[69] Wang J. Assessment of the amide-I local modes in gamma- and beta-turns of peptides, Physical Chemistry and Chemical Physics 2009;11:5310-5322.

[70] Cances E, Mennucci B, Tomasi J. A new integral equation formalism for the polarizable continuum model: Theoretical background and applications to isotropic and anisotropic dielectrics. The Journal of Chemical Physics 1997;107:3032-41.

[71] Wang J. Ab initio-based all-mode two-dimensional infrared spectroscopy of a sugar molecule. The Journal of Physical Chemistry B 2007;111:9193-96.